Different approaches to handling vertical and streamwise sorting in modeling river morphodynamics

Astrid Blom[1,2]

Received 29 August 2006; revised 14 November 2007; accepted 11 December 2007; published 15 March 2008.

[1] This paper presents an assessment of the strengths and weaknesses of four sediment continuity models for nonuniform sediment by applying these models to an aggradational flume experiment that is dominated by nonuniform sediment and dunes. The author makes simulations of the flume experiment using four numerical morphodynamic model systems to which the following sediment continuity models are applied: the commonly applied active layer model (A), a two-layer model (B), a sorting evolution model while assuming bed form size to be regular (C1), and a sorting evolution model while taking into account the variability in bed form geometry (C2). The model systems that incorporate the variability of bed form geometry, i.e., the two-layer model and the sorting evolution model with irregular dunes, show an improved prediction of the adaptation timescale of the composition of both the bed surface and the transported sediment, as well as the vertical sorting profile. This is because including the variability of bed form geometry enables the model system to account for sediment being stored (temporarily) at elevations that are exposed to the flow less frequently. Future application of both models to field cases is difficult, however, as the two-layer model is not sufficiently generic and may lead to ellipticity of its set of equations, whereas the sorting evolution model requires a very small numerical time step.

Citation: Blom, A. (2008), Different approaches to handling vertical and streamwise sorting in modeling river morphodynamics, *Water Resour. Res.*, *44*, W03415, doi:10.1029/2006WR005474.

1. Introduction

[2] We use morphodynamic model systems in order to gain insight into, for instance, the long-term morphodynamic changes of a river system. Here a morphodynamic model system is defined as a system that couples modules for calculating flow, hydraulic roughness, sediment transport, and morphodynamic changes. If sediment sorting processes are significant, the model system needs to include a sediment continuity model describing the interaction among grain size–selective sediment transport, the vertical sorting profile, and net aggradation or degradation of the river bed. The purpose of such a sediment continuity model for nonuniform sediment is to take into account the effects of grain size–selective sediment transport and sorting in modeling large-scale morphodynamic changes of the river bed.

[3] *Hirano* [1971] was the first to develop such a sediment continuity model for nonuniform sediment, and proposed representing the active part of the bed as a distinct and homogeneous surface layer, i.e., the active layer. This active layer reflects the part of the bed that is exposed to and interacts with the flow, and is thus subject to entrainment and deposition. As such, it represents the part of the bed that, jointly with the flow, determines the rate and composition of the transported sediment. From a modeling perspective, the active layer is defined in order to determine a representative grain size of the bed surface. This representative grain size of the bed surface is required as input for calculating skin friction, bed load transport, and suspended load transport. *Blom and Parker* [2004] summarize the additions to the Hirano active layer model as proposed by various researchers.

[4] In the Hirano active layer model vertical sediment fluxes arise from net aggradation or degradation only. From observations, however, we know that the migration of bed forms in itself causes sediment to become redistributed over the active elevations of the bed. Avalanching of grains down a bed form lee face results in a downward coarsening trend within bed forms [e.g., *Bagnold*, 1941; *Allen*, 1965; *Zanke*, 1976], also in situations without net aggradation or degradation. Moreover, the occurrence of relatively deep troughs in a series of irregular bed forms leads to vertical sediment fluxes between the upper part of the active bed and deeper elevations that are less exposed to the flow. Similar to the work by *Crickmore and Lean* [1962a, 1962b] for tracer particles, *Ribberink* [1987] introduced an additional layer into the active layer model, i.e., the exchange layer, in order to account for the effects of the variability in trough elevations. Another shortcoming of the Hirano active layer model, and to a less extent of the Ribberink two-layer model, is that the set of equations can become elliptic in parts of the space-time

[1]Water Engineering and Management, University of Twente, Enschede, Netherlands.
[2]Now at Environmental Fluid Mechanics Section, Civil Engineering and Geosciences, Delft University of Technology, Delft, Netherlands.

0043-1397/08/2006WR005474$09.00

domain in a situation of net degradation into a substrate that is finer than the active layer [*Ribberink*, 1987]. This indicates that in such a situation the bed layer models fail to describe the actual physical processes. Modeling degradation into a fine substrate leads to an unrealistically rapid exchange of sediment between the homogeneous bed layers, which appears to be the cause of the ellipticity.

[5] *Armanini* [1995] pointed out that the discrete active layer is an oversimplification of reality and that this zone of finite thickness where instantaneous and complete mixing occurs does not exist. He was the first to abandon the concept of discrete bed layers. *Armanini*'s [1995] depth-continuous model describes the time evolution of vertical sediment fluxes and the composition of the bed material at each elevation of the bed. The vertical sediment fluxes are modeled as a diffusion process, in which fine and coarse size fractions do not show any preference for being deposited at specific bed elevations. As such, the equilibrium state of the model, which is reached after an infinitely long time, is a vertically uniform distribution of grain sizes, which does not agree with experimental observations [e.g., *Ribberink*, 1987; *Blom et al.*, 2003].

[6] *Parker et al.* [2000] developed a new type of framework for sediment continuity and sorting dynamics. Like *Armanini* [1995], they recognize that the active layer model and its variants represent only an approximation of a more general formulation that contains no discrete bed layers. In this new framework, the bed composition varies continuously over depth below the water-sediment interface, and the same goes for the entrainment and deposition fluxes from and to the bed. A probability density function (PDF) of bed surface elevations is the basis of the framework, which allows us to take into account that relatively deep bed elevations are exposed to the flow and are subject to entrainment and deposition less frequently than higher ones.

[7] *Blom and Parker* [2004] derive formulations for the grain size–specific and bed elevation–specific entrainment and deposition fluxes required for the *Parker et al.* [2000] framework, for situations dominated by river dunes and bed load transport. Here *Knighton*'s [1998] definition of dunes is applied; bed forms with a length of 4 to 8 times the flow depth and a height of up to a third of the flow depth are classified as dunes. The main sorting mechanism within dunes is the avalanching of grains down the lee faces of bed forms with varying trough elevations [e.g., *Ribberink*, 1987; *Blom et al.*, 2003]. In order to cover this mechanism, *Blom and Parker* [2004] combine a submodel describing the sorting due to the avalanching of grains down the lee faces of individual bed forms with a stochastic approach characterizing the variability in bed form size. Characteristics of the flow over the bed form crest (as well as flow separation and the wake) have appeared not to significantly affect the sorting due to grain avalanches [*Blom and Kleinhans*, 2006].

[8] *Blom et al.* [2006] reduce the *Blom and Parker* [2004] continuum model to equilibrium conditions, i.e., conditions in which all variables vary in time around steady mean values. We can apply this equilibrium sorting model in a morphodynamic model system instantaneously if the timescale of large-scale morphodynamic changes (i.e., net aggradation or degradation) is much larger than both the timescale of vertical sorting and the timescale of the evolution of the PDF of trough elevations.

[9] Following the equilibrium sorting model, *Blom et al.* [2008] develop a sorting evolution model in order to take into account the time evolution of the sorting profile in predicting large-scale river morphodynamics. Morphodynamic models that are set up for analyzing, for instance, the long-term morphodynamic changes and sorting within a river system usually cover several tens of kilometers of river length or more. Such models are often (but not necessarily) simplified to one-dimensional models, which means that lateral and vertical flow variations are not considered, or only in a parameterized way. In such models the streamwise size of a grid cell may well be several hundreds of meters or larger. Up to now, in such computations the active part of the bed has been represented by a discrete and homogeneous active layer. The sorting evolution model by *Blom et al.* [2008] describes the active part of the bed in a stochastic and nonhomogeneous way, which offers a better representation of the active part of the bed.

[10] *Blom et al.* [2008] apply the sorting evolution model to conditions that vary in the vertical direction only. This paper describes the application of the sorting evolution model to a flume experiment in which conditions also vary in the streamwise direction. In the flume experiment in question, a phase of net aggradation succeeds a short phase of net degradation. As the purpose of a sediment continuity model for nonuniform sediment is to take into account the effects of grain size–selective transport and vertical sorting in predicting large-scale aggradation and degradation of the river bed, which by definition involve streamwise variation, the present case study provides a relevant test of the sorting evolution model.

[11] We can analyze the performance of a sediment continuity model in simulating such a flume experiment only after implementing it in a morphodynamic model system. The author makes simulations using four numerical morphodynamic model systems to which the following sediment continuity models are applied: the *Hirano* [1971] active layer model (A), the *Ribberink* [1987] two-layer model (B), the *Blom et al.* [2008] sorting evolution model with regular dunes (C1), and the *Blom et al.* [2008] sorting evolution model with irregular dunes (C2).

[12] The specific objective of this case study is the assessment of the strengths and weaknesses of submodels for sediment continuity. The author therefore reduces other submodels in the morphodynamic model systems as much as possible. For instance, we use measured data rather than predictive submodels whenever possible. The author assesses the four morphodynamic model systems in simulating the aggradational flume experiment conducted by *Ribberink* [1987], and compares the predictions to measured data with respect to the composition of the active part of the bed, (grain size–selective) sediment transport rates, mean bed level, vertical sorting, and the accompanying timescales.

[13] Section 2 describes the aggradational flume experiment. Section 3 presents an overview of the submodels applied in the four morphodynamic model systems, as well as the initial and boundary conditions. In section 4 we compare the results of the computations to measured data.

2. Flume Experiment

[14] The author applies the four morphodynamic model systems in simulating a flume experiment in which (1)

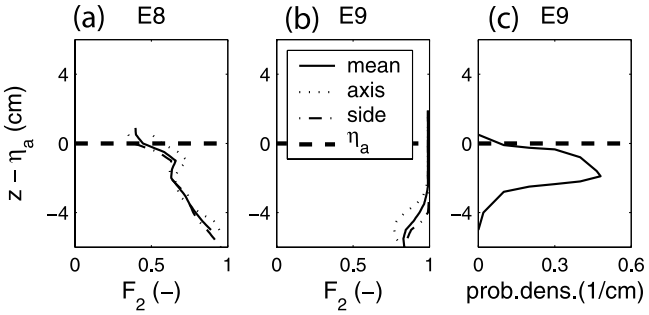

Figure 1. Data measured by *Ribberink* [1987] on (a) variation of the volume fraction content of the coarse size fraction, F_2, over bed elevations at the initial stage of experiment E8–E9 (E8); (b) variation of the volume fraction content of the coarse size fraction over bed elevations at the final stage (E9); and (c) probability density of measured relative trough elevations at the final stage (E9). Here η_a denotes mean bed level and z denotes bed elevation. Figures 1a and 1b show vertical sorting profiles averaged over samples taken at the axis of the flume and over samples taken at the sides of the flume as well as the mean sorting profile. Dashed lines indicate the mean bed level at the corresponding stage of the experiment.

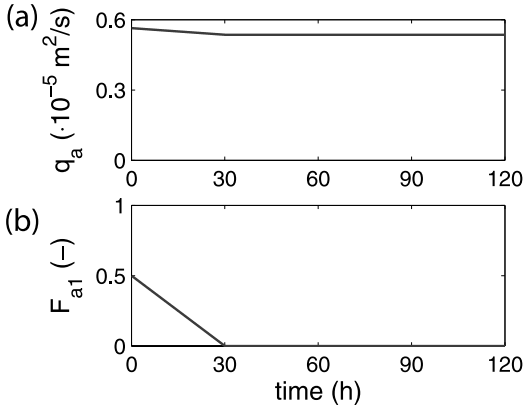

Figure 2. (a) Time evolution of the imposed sediment feed rate, q_a, at the upstream end of the flume ($x = 0$ m). Because of technical problems, the total feed rate decreased by about 5% over the first 30 h of the flume experiment. (b) Time evolution of the imposed volume fraction content of the fine size fraction, F_{a1}, in the sediment fed at the upstream end of the flume. Data originate from *Ribberink* [1987].

mixed-size sediment was used; (2) conditions with dunes prevailed; (3) net aggradation or degradation occurred; and (4) the vertical sorting profile was measured. As far as known to the author, *Ribberink* [1987] has been the only one who conducted such a flume experiment (i.e., experiment E8-E9).

[15] The length, width, and height of the flume's measurement section were 30 m, 0.3 m, and 0.5 m, respectively. The sediment mixture consisted of two sand fractions (grain sizes $d_1 = 0.78$ mm, $d_2 = 1.29$ mm) with very little overlap. Although the difference in grain size is relatively small, the difference between the transport dynamics of the two size fractions is significant and is expressed by the preferential entrainment of the fine size fraction and by the downward coarsening trend over the active part of the bed. *Ribberink* [1987] took bed samples using sampling pipes pressed into the bed near the bed form crests. Through the sampling pipes, he removed sand layers with a thickness of 0.5 cm by siphon. He dried and sieved the small subsamples, and restored the bed by returning the subsamples in reverse order to keep the disturbance of the bed as small as possible. Unfortunately, information on how many bed samples were used in determining the average sorting profile corresponding to stage E8 or stage E9 is no longer available.

[16] Experiment E8-E9 started from the equilibrium stage of the previous experiment, i.e., experiment E8. A downward coarsening trend characterizes the initial vertical sorting profile (Figure 1a).

[17] In experiment E8-E9 the water discharge was maintained steady and was equal to the water discharge in experiment E8. The level of the weir at the downstream end of the flume was equal to the one in experiment E8.

[18] Whereas *Ribberink* [1987] applied sediment recirculation in the previous experiments, from the start of experiment E8-E9 he used a sediment feed system. The initial feed rate was equal to the equilibrium sediment transport rate and composition as measured in experiment E8. Then, over a period of 30 h, *Ribberink* [1987] gradually reduced the volume fraction content of the fine size fraction in the sediment fed to the flume to 0 (Figure 2b), while the total feed rate was maintained steady (Figure 2a). Because of technical problems, the total feed rate decreased by about 5% over the first 30 h of the flume experiment (Figure 2a). The duration of the experiment was 120 h.

[19] Because of the imposed increase of coarse sediment fed to the flume, the active part of the bed started to coarsen at the upstream end of the flume. As a result, the sediment transport capacity decreased and a small degradation wave migrated in the downstream direction. As the total feed rate was steady, an aggradation wave succeeded the small degradation wave (Figure 3). Figure 3 shows the time evolution of the measured mean bed level, η_a, during experiment E8-E9 at two positions along the flume. We can identify a phase lag between the two positions; the minimum bed level was

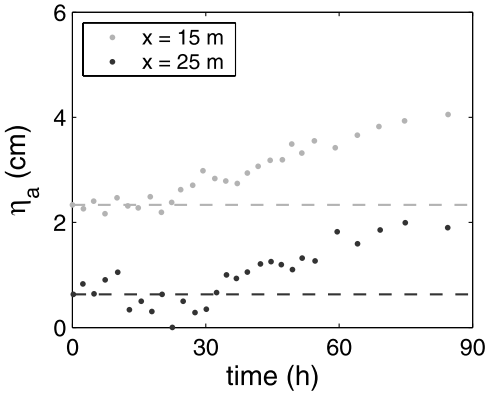

Figure 3. Time evolution of the measured mean bed level, η_a, during experiment E8-E9 at two positions along the flume. Dashed lines indicate the mean bed level at the initial stage of the experiment at the two corresponding positions. The position $x = 0$ m corresponds to the upstream end of the flume. Data originate from *Ribberink* [1987].

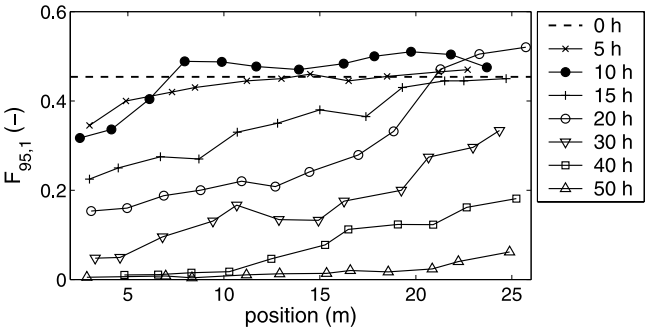

Figure 4. Measured volume fraction content of the fine size fraction in the active part of the bed, F_{95i}, as a function of the position along the flume at various times. Data originate from *Ribberink* [1987].

reached between 0 and 20 flow hours for x = 15 m, and between 15 and 30 flow hours for x = 25 m.

[20] *Ribberink* [1987] estimated the composition of the active part of the bed by averaging over all bed material above the elevation η_{95}. Here η_{95} denotes the elevation above which 95% of the bed surface elevations occur ($P_s(\eta_{95}) = 0.95$, where P_s denotes the probability distribution of bed surface elevations). Figure 4 shows the measured volume fraction content of the fine size fraction in the active part of the bed, F_{95i}, as a function of the position along the flume at various times during the flume experiment. The data in Figure 4 stems from smoothing the original data using a moving average in order to reduce the large natural spatial fluctuations [*Ribberink*, 1987]. Figure 4 shows that, because of the coarse sediment feeding, the active part of the bed coarsened at the upstream end of the flume and a coarsening wave migrated in the downstream direction through the flume.

[21] Figure 4 also illustrates that around 10 flow hours the active part of the bed is somewhat finer than the original situation. *Ribberink* [1987] indicated two possible causes for this relative fining: (1) the temporary reduction in dune height between 5 and 10 flow hours, which caused the vertically averaged composition of the active bed, F_{95i}, to be based on the upper, relatively fine, part of the bed, and (2) the large spatial variations in composition in combination with the relatively low number of bed samples, which resulted in a large statistical inaccuracy. Another possible explanation, however, is that a small fining wave migrated in the downstream direction, preceding the distinct coarsening wave. This fining wave may be caused by an increase of the mobility of the fine sediment where the bed, because of the coarse sediment feeding, coarsened. Observation of an increase in the mobility of fine sediment due to an increased amount of coarse sediment is very uncommon but was observed earlier by *Gilbert* [1914] and *Ikeda and Iseya* [1988]. *Gilbert* [1914] mentioned two reasons for the increased mobility of fines due to a larger amount of coarse particles. The first reason is the impact of the coarser particles: "In rolling and leaping they disturb the finer, tending thus to dislodge them from their resting places and either start them forward or else give them new positions from which they may be more easily swept" [*Gilbert*, 1914, p. 178]. The second reason is the production of diversity in the current by the coarser grains. By obstructing the flow, the coarse grains cause zones of flow deceleration and acceleration, which gives rise to a higher mobility of the fines. *Gilbert* [1914] underlined the uncommonness of an increase in the mobility of fines due to an increased amount of coarse material, as under most conditions an increased amount of coarse material results in a decrease of the mobility. Unfortunately the author is not able to analyze the cause of the relative fining in detail as original data on the vertical sorting profiles and bed and water elevation profiles are lacking.

[22] Figure 1b shows the vertical sorting profile as measured at the final stage of experiment E8-E9. The upper part of the bed consisted of the coarse size fraction only. At the sides of the flume the coarsening reached deeper elevations than at the axis of the flume. This was because at the sides vertical sediment fluxes reached deeper elevations, as at the sides troughs were deeper than in the axis of the flume [*Ribberink*, 1987]. This lateral variation in trough elevation may be due to secondary currents that originate from wall friction.

[23] Figure 1c shows the PDF of trough elevations relative to the mean bed level for a series of bed forms at the final stage of experiment E8-E9. This PDF of relative trough elevations indicates the probability density that the trough elevation equals $z - \eta_a$, where η_a denotes the mean bed level. Unfortunately, the PDF of measured relative trough elevations from the initial stage of the experiment is not available anymore, nor the original bed elevation profiles. Comparison of Figures 1a–1c shows that the lower limit of trough elevations in E9 ($\Delta_b = \eta_a - z \approx 5$ cm) more or less agrees with the lower boundary of the range of bed elevations that have been reworked during experiment E8-E9.

3. Details of the Four Model Systems

3.1. Setup of the Model Systems

[24] The case study described in the present paper considers four numerical morphodynamic model systems. Models A and B are morphodynamic model systems to which the *Hirano* [1971] active layer model and the *Ribberink* [1987] two-layer model are applied, respectively. Appendices A and B provide a brief explanation of these two sediment continuity models. The sorting evolution model developed by *Blom et al.* [2008] is the basis of models C1 and C2. Appendix C provides a short description of the sorting evolution model, and explains how the sorting evolution model distinguishes three types of vertical sediment fluxes: sediment fluxes through dune migration, i.e., grain size–selective deposition through avalanching down the lee faces of (irregular) bed forms (type I); sediment fluxes through a change in time of the PDF of relative trough elevations (type II); and sediment fluxes through net aggradation or degradation (type III). In model C1, the author imposes bed form size to be regular, whereas model C2 accounts for the variability in bed form size. Models C1 and C2 differ with respect to the shape of the PDF of relative bed form trough elevations. This PDF of trough elevations is required in the computation of sediment fluxes through dune migration (type I). In model C1, the PDF of trough elevations reduces to a Dirac delta function with a single dominant

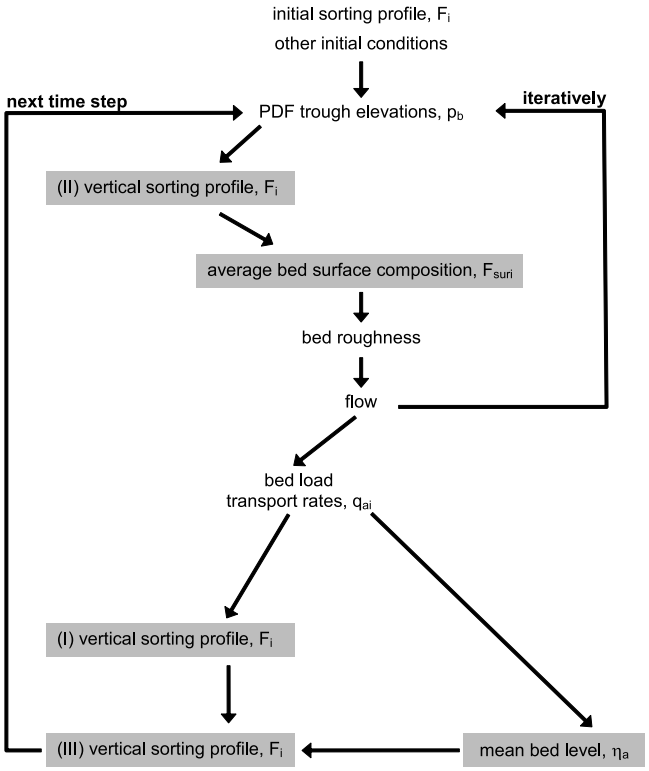

Figure 5. Scheme of the morphodynamic model system for nonuniform sediment to which the sorting evolution model is applied. Gray boxes represent submodels that are part of the sorting evolution model. Evolution of the vertical sorting profile occurs through vertical sediment fluxes accompanying migration of bed forms of irregular size (type I), a change in time of the PDF of relative trough elevations (type II), and net aggradation or degradation (type III).

trough elevation. Model C2 applies the PDF of measured relative trough elevations as input to the model system. Section 3.3 explains this difference in further detail.

[25] As the purpose of a sediment continuity model for nonuniform sediment is to account for the effects of grain size–selective transport and vertical sorting in predicting large-scale aggradation and degradation of the river bed, it is applied over spatial scales that cover a large number of bed forms. This means that each grid point in the morphodynamic model system covers a large number of bed forms, and implies that most input and output parameters of the model are averaged over a reach covering a large number of bed forms.

[26] Figure 5 illustrates how the morphodynamic model system incorporates the sorting evolution model. On the basis of a set of initial conditions, the model system determines the PDF of relative trough elevations at the next time step using either measured data or a submodel for the PDF of relative trough elevations. A change in time of the PDF of relative trough elevations results in vertical sediment fluxes of type II, which affect the vertical sorting profile. This leads to a change in time of the mean composition of the bed surface, F_{suri}, which influences the grain roughness or skin friction. The PDF of relative trough elevations affects the form roughness or form drag. Skin friction and form drag together determine the bed resistance, which affects the flow. The above quantities may be solved iteratively. From the flow properties and the mean bed surface composition, the model system then determines the grain size–selective bed load transport rates, q_{ai}, using a submodel for grain size–selective sediment transport.

[27] Bed load transport is here accompanied by the migration of (irregular) dunes, which induces vertical sediment fluxes of type I and adaptation of the vertical sorting profile, F_i (Figure 5). Divergences in the total sediment transport rate, i.e., variations in the total sediment transport rate in the streamwise direction, lead to a change in time of the mean bed level, η_a, which gives rise to vertical sediment fluxes of type III and adaptation of the vertical sorting profile, F_i. This completes the computational steps within one cycle of the model system, thus closing the loop in Figure 5.

[28] The model systems based on the Hirano active layer model and the Ribberink two-layer model (models A and B, respectively) also follow the scheme presented in Figure 5. Application of the Hirano model asks for the following changes to the scheme: (1) a homogeneous active layer represents the active part of the bed rather than a PDF of trough elevations; (2) a change in time of the active layer thickness induces vertical sediment fluxes of type II; and (3) vertical sediment fluxes of type I (i.e., due to dune migration) do not occur. Application of the Ribberink model asks for the following changes: (1) an active layer and an exchange layer represent the active part of the bed rather than a PDF of trough elevations; (2) a change in time of the active layer thickness and exchange layer thickness induces vertical sediment fluxes of type II; and (3) vertical sediment fluxes of type I (i.e., due to dune migration) occur through the sediment exchange term ψ_i (see Appendix B).

[29] As the present case study focuses on modeling sediment continuity, we reduce other submodels in Figure 5 as much as possible. For instance, we use measured data rather than predictive submodels for the hydraulic roughness, the PDF of relative trough elevations, and dune height. Besides, we apply a sediment transport model that was calibrated against the flume experiments.

3.2. Boundary Conditions

[30] The water discharge per unit width, q_w, at the upstream end (x = 0 m) is steady and equals 0.0803 m^2/s. The water level, h, at the downstream end (x = 30 m) is steady and equals 0.167 m. The sediment feed rate at the upstream end of the flume, q_s, equals $5.64 \cdot 10^{-6}$ m^2/s at $t = 0$. The feed rate decreases by about 5% over the first 30 h of the flume experiment (Figure 2a). The imposed upstream volume fraction of the fine size fraction decreases from 0.5 to 0 over the first 30 h of the experiment (Figure 2b).

3.3. Active Part of the Bed

[31] The active layer thickness, δ, in models A and B is a function of the mean bed form height: $\delta = \frac{1}{2}\Delta$ [*Ribberink*, 1987; *Armanini and Di Silvio*, 1988; *Parker*, 1991]. During the experiment the mean dune height decreased from 3.3 to 2.9 cm. In the present case study, the author assumes dune height to be steady (Δ = 3 cm). Following *Ribberink* [1987], the thickness of the exchange layer, δ_e, in the

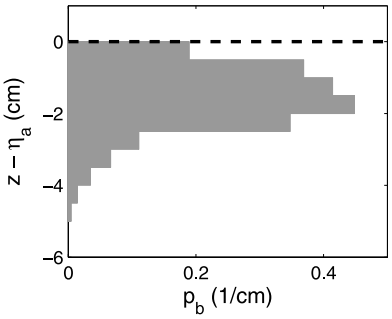

Figure 6. PDF of measured relative trough elevations (stage E9) weighted by the horizontal distance involved, $\tilde{p}_b$. The dashed line indicates the mean bed level at the corresponding stage of the experiment. This PDF of relative trough elevations is used as input in model C2.

two-layer model is a function of the active layer thickness ($\delta_e = 1.22\delta$).

[32] In the sorting evolution model with regular dunes (model C1), the PDF of relative trough elevations reduces to the Dirac delta function, in which the dominant relative trough elevation, Δ_b, follows from the mean dune height, Δ: $\Delta_b = \frac{1}{2}\Delta$. This results in the same lower boundary of the active part of the bed as in model A, the Hirano model. In model C2, the PDF of relative trough elevations as measured in stage E9 represents the variation in relative trough elevations (Figure 1c). This PDF of relative trough elevations is adapted by weighting each trough elevation by the horizontal distance involved [*Blom and Parker*, 2004, equation (56)]. Moreover, trough elevations above the mean bed level have been neglected as the crest of an individual bed form is assumed to be located the same distance above the mean bed level as its trough is located below the mean bed level. The PDF is discretized into 10 relative trough elevations (Figure 6). The author assumes the PDF of relative trough elevations, $\tilde{p}_b$, in Figure 6 to be valid for the complete experiment.

[33] When analyzing the results in the next section, it is important to realize that [*Ribberink*, 1987] estimated the measured composition of the active part of the bed, $F_{95\,i}$, by averaging over all bed material above the elevation η_{95} (also see section 2). The original vertical sorting data from which $F_{95\,i}$ was computed is not available anymore. The author conveniently uses the same definition for the composition of the active bed in analyzing the results of the sorting evolution model (model C). Yet, in the case of the non-probabilistic Hirano and Ribberink models, we can only compare the measured data for $F_{95\,i}$ to the predicted composition of the active layer, F_{mi}:

$$F_{95\,i} = \begin{cases} F_{mi} & \text{(models A, B)} \\ \dfrac{\int_{\eta_{95}}^{\infty} F_i P_s\, dz}{\int_{\eta_{95}}^{\infty} P_s\, dz} & \text{(measured data, model C)} \end{cases} \tag{1}$$

where the probability distribution of bed surface elevations, P_s, is a function of the PDF of bed surface elevations, p_e:

$$P_s = 1 - \int_{-\infty}^{z} p_e dz \tag{2}$$

and where p_e is a function of the PDF of relative trough elevations, $\tilde{p}_b$ (Figure 6):

$$p_e = \int_{\eta_{b\min}}^{\eta_{b\max}} \frac{J}{\Delta}\, \tilde{p}_b\, d\eta_b \tag{3}$$

Here η_b denotes the bed form trough elevation, $\eta_{b\min}$ denotes the lowest trough elevation, and $\eta_{b\max}$ denotes the highest trough elevation. The Heaviside function J equals 1 when considering an elevation covered by the specific bed form.

[34] It is important to realize that the PDF of relative trough elevations indicates the range of elevations representing the active part of the bed for the sorting evolution model, just as the bed form height indicates the range of elevations representing the active part of the bed for the Hirano and Ribberink models. For all four models the information on the range of active elevations is taken from measured data.

3.4. Initial Conditions

[35] The initial state of flume experiment E8-E9 is an equilibrium state (E8). The initial flow profile is spatially uniform with a water depth equal to 0.167 m. The initial bed slope, s_0, equals $1.65 \cdot 10^{-3}$. The initial vertical sorting profile equals the vertical sorting profile as measured in the equilibrium stage of experiment E8 (Figure 1a).

[36] Models A and B require information on the initial composition of the homogeneous active layer, $F_{mi}(t = 0)$. To this end, we average the measured initial sorting profile, F_i, over all bed material above the lower boundary of the active layer:

$$F_{mi}(t = 0) = \frac{\int_{\eta_a - \delta}^{\infty} F_i P_s\, dz}{\int_{\eta_a - \delta}^{\infty} P_s\, dz} \tag{4}$$

This results in $F_{m1} = 0.45$ and $F_{m2} = 1 - F_{m1} = 0.55$.

[37] Likewise, model B requires information on the initial composition of the homogeneous exchange layer, $F_{ei}(t = 0)$. For this purpose, we average the measured initial sorting profile over all bed material at the bed elevations covered by the exchange layer:

$$F_{ei}(t = 0) = \frac{\int_{\eta_a - \delta - \delta_e}^{\eta_a - \delta} F_i P_s\, dz}{\int_{\eta_a - \delta - \delta_e}^{\eta_a - \delta} P_s\, dz} \tag{5}$$

This results in $F_{e1} = 0.32$ and $F_{e2} = 1 - F_{e1} = 0.68$.

[38] For models C1 and C2, the initial sorting profile equals the sorting profile as measured in experiment E8 (Figure 1a). We assign the uppermost elevations that are active according to the PDF of bed surface elevations but for which no measured data on the composition are available the same composition as the uppermost elevation with a measured initial composition.

3.5. Hydraulic Roughness

[39] We assume the hydraulic roughness (i.e., the sum of skin friction, form drag, and wall roughness) to be steady and uniform (Chézy roughness coefficient $C = 28.9\ \mathrm{m}^{1/2}/\mathrm{s}$) [*Ribberink*, 1987]. This Chézy value results in a uniform flow in the initial stage of the experiment ($h = 0.167$ m, E8).

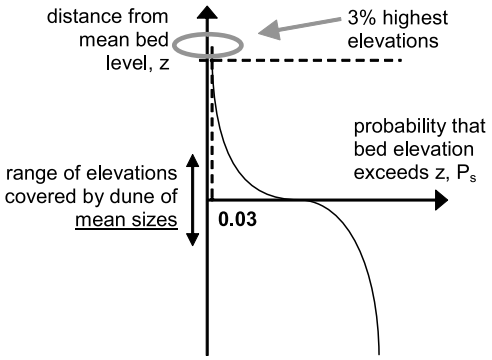

Figure 7. The 3% highest elevations within the series of (irregular) bed forms, which are not considered in the computations using model C.

3.6. Flow

[40] Simplification of the Navier-Stokes equations to the case of nonsteady nonuniform 1D shallow open channel flow results in the St Venant Shallow Water equations, which for steady gradually varied flow reduce to the formulation for a backwater curve [e.g., *Hotchkiss and Parker*, 1991]. The experimental setup (i.e., a steady water discharge at the upstream end, a steady weir level at the downstream end, no lateral variations) means that the flow is well described using the general formulation for a backwater curve.

3.7. Sediment Transport

[41] *Ribberink* [1987] calibrated an adapted version of the *Meyer-Peter and Müller* [1948] sediment transport model (including the hiding-exposure correction by *Egiazaroff* [1965]) against the equilibrium stages of the complete set of 9 flume experiments. *Ribberink* [1987] provides a full description of the resulting sediment transport model. As the specific focus of this case study is the assessment of submodels for sediment continuity, the author uses the *Ribberink* [1987] modification of the *Meyer-Peter and Müller* [1948] sediment transport model, so as to reduce the uncertainties inherent to using a sediment transport model and to reduce the effects of deviations in the predicted sediment transport rates from the actual sediment transport rates on the computational results.

[42] The resulting grain size–selective sediment transport submodel is a function of both the volume fraction content of size fraction i at the bed surface, F_{suri} (i.e., the mean bed surface composition), and the geometric mean grain size of the bed surface, d_{msur}, which by itself also depends on F_{suri}. The next section presents the details of the models for the bed surface composition, F_{suri}, and the geometric mean grain size of the bed surface, d_{msur}.

3.8. Bed Surface Composition

[43] Sediment transport rates and skin friction usually depend on the bed surface composition, F_{suri}. When using the Hirano active layer model (model A) or the Ribberink two-layer model (model B), we assume the bed surface composition to be equal to the composition of the active layer, F_{mi}. In model C, the mean composition of the bed surface is equal to the actual composition of the surface of the bed. More specifically, when applying the sorting evolution model (model C), we compute the mean bed surface composition, F_{suri}, by weighting the bed composition F_i by the probability density that elevation z is exposed to the flow, p_e [*Blom et al.*, 2008]:

$$F_{suri} = \begin{cases} F_{mi} & \text{(models A, B)} \\ \int_{-\infty}^{\infty} F_i\, p_e\, dz & \text{(model C)} \end{cases} \tag{6}$$

[44] We compute the geometric mean grain size of the bed surface, d_{msur}, from

$$d_{msur} = d_{ref}\ 2^{-\phi_{msur}} \tag{7}$$

where the geometric reference grain size, d_{ref}, equals 1 mm, and the arithmetic mean grain size of the bed surface, ϕ_{msur}, equals

$$\phi_{msur} = \sum_{i}^{N} F_{suri}\, \phi_i \tag{8}$$

where ϕ_i is the arithmetic grain size of size fraction i:

$$\phi_i = -\log_2\left(d_i/d_{ref}\right) \tag{9}$$

where d_i denotes the geometric grain size of size fraction i. The definition in equation (9) makes the arithmetic grain size ϕ_i correctly dimensionless.

3.9. Numerical Parameters

[45] In models A and B, the time step Δt equals 5 min. In models C1 and C2, the time step equals 20 s in the computation of sediment fluxes of type I and 1 min in the computation of sediment fluxes of type III. Sediment fluxes of type II do not occur as bed form geometry and the PDF of relative trough elevations are steady. The horizontal spatial step, Δx, equals 1 m (all models). The vertical spatial step, Δz, equals 1 mm (all models). The vertical grid ranges from below the lower elevation of the active part of the bed up to above its upper elevation. We apply a "bookkeeping" system to register the time evolution of the volume fraction content of size fractions at elevations within the active and inactive part of the bed. The author applies a predictor-corrector scheme in calculating the backwater curve, and an upwind scheme (upwinding coefficient 0.8) in calculating the bed evolution.

[46] *Blom et al.* [2008] have shown that the timescale of adaptation of the vertical sorting profile through dune migration (sediment fluxes of type I) approaches zero at the uppermost elevations of the active part of the bed. As such, at these elevations the adaptation of the sorting profile happens infinitely fast, which leads to numerical problems. In order to deal with this problem, the author does not consider the 3% highest elevations within the series of (irregular) bed forms, which is illustrated in Figure 7. These 3% highest elevations are elevations that are seldom reached by the bed forms as they are located far above the range of elevations covered by a dune of mean sizes. As such, they have negligible influence on the bed surface composition and skin friction.

3.10. Adjustment Period

[47] Numerical simulations of time-dependent processes often require an adjustment period in order to find a

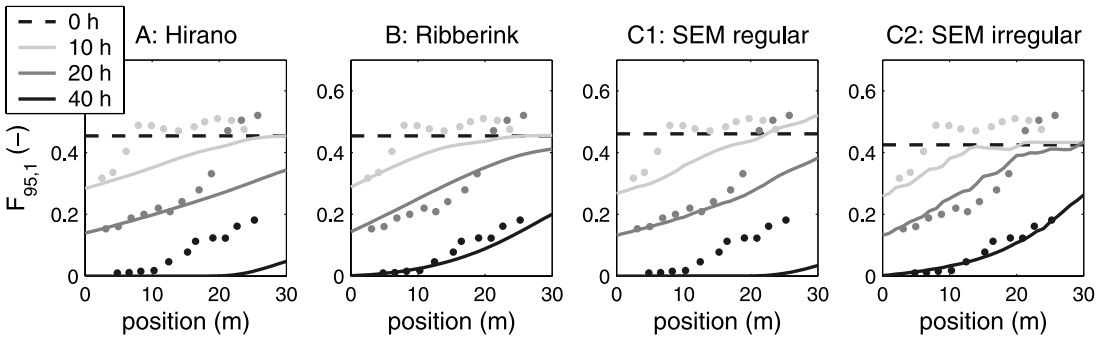

Figure 8. Volume fraction content of the fine size fraction in the active part of the bed, F_{95i}, as a function of the position along the flume at various times (T = 0 h, T = 10 h, T = 20 h, and T = 40 h). Predictions (lines) are from (left to right) model A, the Hirano active layer model; model B, the Ribberink two-layer model; model C1, the sorting evolution model with regular dunes; and model C2, the sorting evolution model with irregular dunes. Measured data (dots) originate from *Ribberink* [1987].

physically relevant initial state for the actual model simulation, i.e., an initial state that suits the initial conditions of the actual model simulation. In this case study the author applies an adjustment period T' (T' = 5 h) in which each simulation, under steady and uniform flow conditions, adjusts toward the equilibrium state that corresponds to the initial conditions. In this way, the actual model simulations show the actual response to the changing boundary conditions (i.e., the imposed coarsening of fed sediment) rather than a complex interplay of adjustments to various factors. Models B, C1, and C2 develop an initial state with respect to the sorting profile that is (close to) its equilibrium state, while the initial state of model A does not deviate from the initial state at the start of the adjustment period.

4. Results

[48] In this section we discuss the results of applying the *Hirano* [1971] active layer model (model A), the *Ribberink* [1987] two-layer model (model B), the sorting evolution model with regular dunes (model SEM C1), and the sorting evolution model with irregular dunes (model SEM C2) to flume experiment E8-E9 conducted by *Ribberink* [1987]. We compare the computational results to the following measured data: (1) the composition of the active part of the bed at various times and positions; (2) the transport rate and volume fraction content of size fractions in the sediment leaving the flume, $q_a(x$ = 28.5 m) and $F_{ai}(x$ = 28.5 m), respectively; (3) the time evolution of the mean bed level, η_a, at various positions; and (4) the vertical sorting profile, F_i, at the final state of the flume experiment. Finally, we assess the sensitivity of the model results to the active layer thickness.

4.1. Composition of the Active Part of the Bed

[49] Figure 8 shows the computed volume fraction content of the fine size fraction in the active part of the bed, at the beginning of the experiment and after 10, 20, and 40 flow hours, compared to the measured data. We have discussed the measured data in section 2 (see Figure 4). Because of the coarse sediment feeding, the active part of the bed coarsens at the upstream end of the flume and a coarsening wave migrates in the streamwise direction through the flume. Although uncertain, preceding the coarsening wave a small fining wave may have migrated in the downstream direction (see section 2). The predicted data show that all models are incapable of simulating the relative fining of the active bed around 10 flow hours. Also application of the *Wilcock and Crowe* [2003] sediment transport model rather than the *Ribberink* [1987] modification of the *Meyer-Peter and Müller* [1948] sediment transport model has not enabled reproduction of this fining.

[50] All models predict the composition of the active part of the bed after 20 flow hours fairly well, except for the relative fining in the downstream part of the flume. After 40 flow hours, only models B and C2 show a good prediction of the active bed composition, while models A and C1 predict the larger part of the fine size fraction to have left the flume. In reality, it apparently takes more time before the fine material leaves the flume, as it is "stored" at relatively deep bed elevations that are exposed to the flow less frequently. Only the Ribberink model (model B) and the sorting evolution model with irregular dunes (model C2) take this aspect into account.

[51] Note that the initial composition of the active bed is slightly different for model C2 (Figure 8). This is due to the larger range of elevations taking part in the active bed. The lower boundary of the active bed in model C2, η_{95}, is located 5 cm below the mean bed level and is lower than the lower boundary of the active bed in models A through C1, i.e., $-\frac{1}{2}\Delta$, which is located 1.5 cm below the mean bed level. This larger range along with the initial downward coarsening trend (Figure 1), makes the initial active bed in model C2 somewhat coarser than in models A through C1.

[52] Figure 9 shows the computed time evolution of the geometric mean grain size of the active bed, d_{m95}, at various positions. We compute the geometric mean grain size of the active bed, d_{m95}, from the volume fraction content of size fraction i in the active part of the bed, F_{95i}, like we compute the geometric mean grain size of the bed surface, d_{msur} from the volume fraction content of size fraction i at the bed surface, F_{suri} (equations (7)–(8)). Figure 9 confirms that incorporating the effects of the irregularities in trough elevations has a significant effect on the timescale of adaptation of the composition of the active bed, and

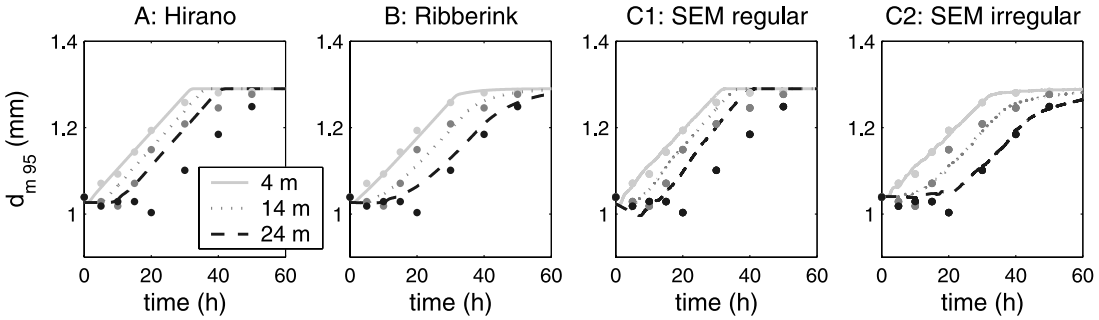

Figure 9. Time evolution of the geometric mean grain size of the active part of the bed, $d_{m\,95}$, at various positions ($x = 4$ m, $x = 14$ m, and $x = 24$ m). Predictions are from (left to right) model A, the Hirano active layer model; model B, the Ribberink two-layer model; model C1, the sorting evolution model with regular dunes; and model C2, the sorting evolution model with irregular dunes. Measured data (dots) originate from *Ribberink* [1987].

illustrates how the sorting evolution model incorporating the effects of irregular bed form size shows the best results in predicting the time evolution of the geometric mean grain size of the bed surface.

4.2. Sediment Transport at Downstream End

[53] Figure 10 shows the time evolution of the sediment transport rate and composition at the downstream end of the flume. The upper plots show the predicted and measured time evolution of the total sediment transport rate at the downstream end of the flume. The imposed coarsening of the sediment fed to the flume induces a coarsening of the bed surface, which decreases the sediment transport rate. The system then evolves toward a state in which it is able to transport the amount and composition of sediment fed to the flume. This results in an increase of the bed slope. All models predict the overall trend fairly well.

[54] The bottom plots in Figure 10 show that models B and C2 well predict the timescale of adaptation of the composition of the transported sediment. Figure 10 shows that including the variability in bed form geometry has a positive effect on the predicted timescale of the physical processes.

[55] The small oscillations in the results of the sorting evolution model (model C) appear to be due to (1) the discretization into 10 trough elevations in model C2 (Figure 6); (2) upper elevations becoming active and lower elevations becoming inactive when the bed aggrades; and (3) the time step of computing sediment fluxes of type III being different from that of type I.

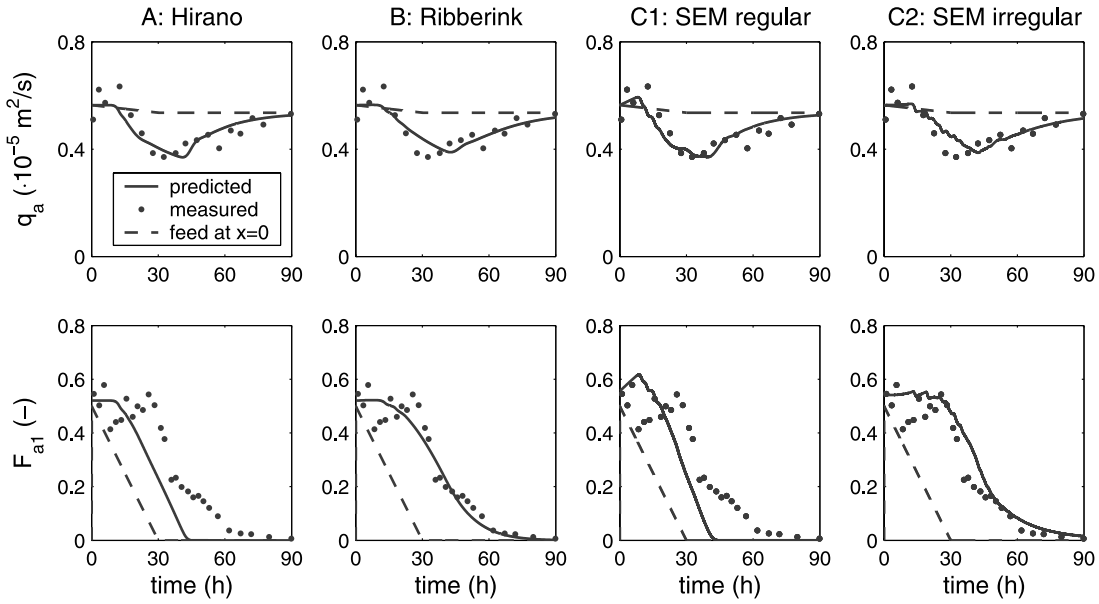

Figure 10. (top) Time evolution of the sediment transport rate, q_a, at the downstream end of the flume ($x = 28.5$ m). (bottom) Time evolution of the volume fraction content of the fine size fraction in the transported sediment, F_{a1}, at $x = 28.5$ m. Predictions (lines) are from (left to right) model A, the Hirano active layer model; model B, the Ribberink two-layer model; model C1, the sorting evolution model with regular dunes; and model C2, the sorting evolution model with irregular dunes. The dashed lines show the feed rate at the upstream end of the flume. Measured data (dots) originate from *Ribberink* [1987].

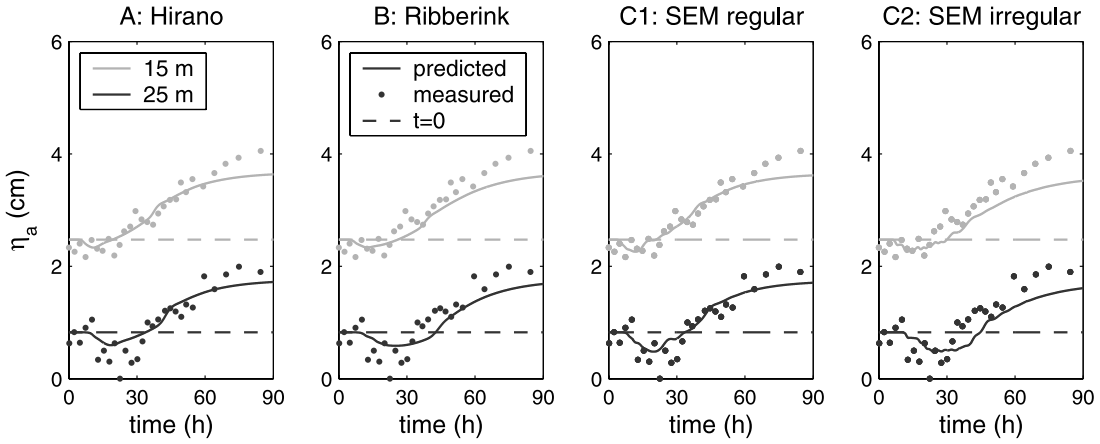

Figure 11. Time evolution of the mean bed level, η_a, at two positions along the flume (x = 15 m and x = 25 m). Predictions (lines) are from (left to right) model A, the Hirano active layer model; model B, the Ribberink two-layer model; model C1, the sorting evolution model with regular dunes; and model C2, the sorting evolution model with irregular dunes. Dashed lines indicate the mean bed level at the initial stage of the experiment at the two corresponding positions. Measured data (dots) originate from *Ribberink* [1987].

4.3. Mean Bed Level

[56] Figure 11 shows the time evolution of the mean bed level at two positions along the flume (x = 15 m and x = 25 m). Section 2 has explained the measured trends. All models reproduce these trends moderately well, although they somewhat underestimate the final amount of net aggradation. *Ribberink* [1987] found that the underestimation of the final amount of aggradation by the Hirano and Ribberink models was due to the fact that the empirical predictors for bed resistance and bed load transport rates were not fully adequate for the conditions of experiment E8-E9. He developed an optimally calibrated model with respect to the mean bed level by adding gradually changing multiplication factors to the submodels for the grain size–specific sediment transport rate and bed resistance. The values of these nonsteady multiplication factors are not available anymore. As the original data on bed and water elevation profiles are not available anymore, it is difficult to reanalyze the exact cause of the underestimation of the final amount of net aggradation.

[57] Figure 12 shows the predicted time evolution of the mean bed slope, together with the measured bed slopes at the initial and final stage of experiment E8-E9. The measured bed slopes were determined over positions downstream of x = 10 m in order to remove the effects of the bed form adaptation length (i.e., the reach from the upstream sediment inlet over which the bed forms adapt to the prevailing conditions). As such, also the predicted mean bed slope was determined over positions downstream of x = 10 m. Four stages can be distinguished. The decrease in bed slope in stage I results from the net degradation at the upstream end of the flume. This decrease in bed slope is succeeded by a significant increase in bed slope (stage II), which originates from the aggradation at the upstream end of the flume. Migration of the aggradation wave in the downstream direction then causes the bed slope to decrease (stage III), which is followed by the new equilibrium stage E9 that ends after 120 flow hours (stage IV). In stage E9 the slope is larger than in E8 so as to enable the system to transport the coarser sediment load.

4.4. Vertical Sorting Profile

[58] Figure 13 shows the time evolution of the vertical sorting profile, F_i, at the downstream end of the flume. The upper plots show the sorting profile at the initial state of the adjustment period T' (also see section 3.10). Section 3.4 has explained how we derive these initial sorting profiles from the measured initial sorting profile as shown in the top right plot in Figure 13. During the adjustment period T', the sorting profiles in models C1 and C2 adjust toward the equilibrium state appropriate to the conditions of experiment E8 (section 3.10). Over its active elevations model C1 has developed a linear sorting profile. This is because the

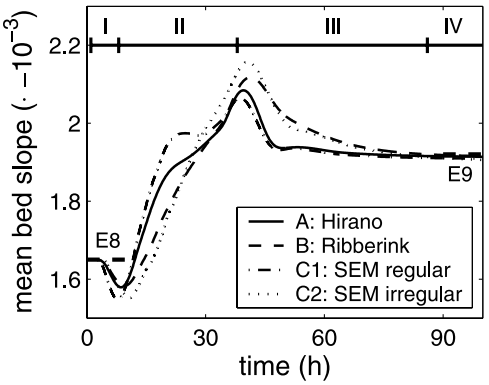

Figure 12. Time evolution of the mean bed slope as predicted by models A through C2. The mean bed slope has been determined over positions along the flume larger than 10 m. Short-dashed lines show the measured bed slopes at the initial and final stage of experiment E8-E9. Four periods are distinguished: decrease of bed slope (period I), increase in bed slope (period II), decrease in bed slope (period III), and the new equilibrium stage (until 120 flow hours) (period IV).

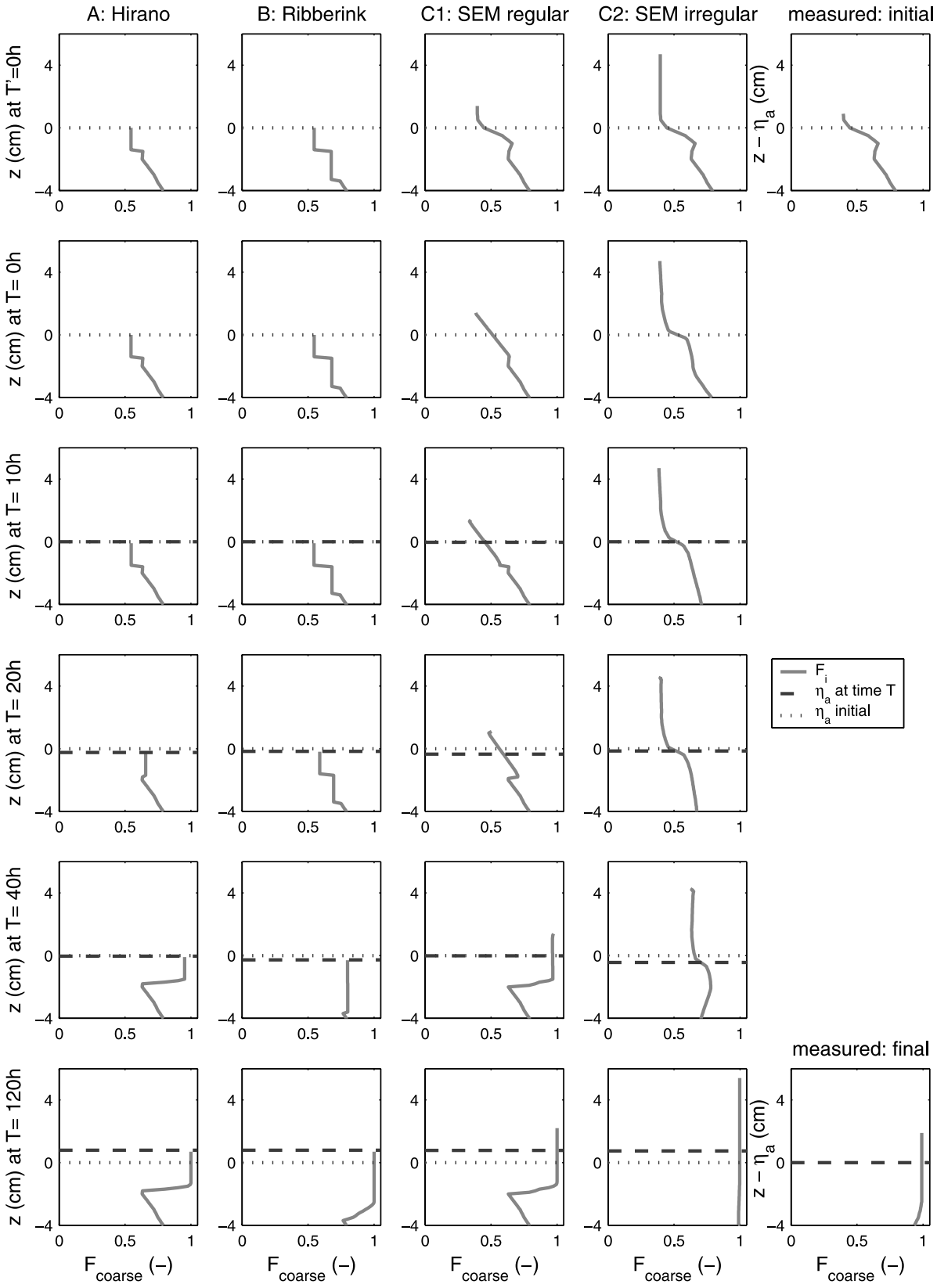
A: Hirano
B: Ribberink
C1: SEM regular
C2: SEM irregular
measured: initial
measured: final
z (cm) at T'=0h
z (cm) at T= 0h
z (cm) at T= 10h
z (cm) at T= 20h
z (cm) at T= 40h
z (cm) at T= 120h
z – η_a (cm)
F_coarse (–)
F_i
η_a at time T
η_a initial

Figure 13

dunes are regular and the lee face avalanche submodel by *Blom and Kleinhans* [2006] applied in the sorting evolution model predicts the volume fraction content of each size fraction to linearly increase or decrease with elevation over the individual lee faces. In model C2, the average vertical sorting profile shows a smoother profile. The second row of plots shows the initial state of the actual simulations of flume experiment E8-E9.

[59] The left plots in Figure 13 show the time evolution of the sorting profile as predicted by the Hirano model (model A). We can see how the active layer becomes coarser, while the bed slowly aggrades.

[60] The second column of plots shows the time evolution of the sorting profile as predicted by the Ribberink model (model B). As in the Hirano model, the active layer becomes coarser, although this process proceeds more slowly than for the Hirano model. Also the exchange layer in the Ribberink model becomes coarser, which proceeds more slowly than the coarsening of the model's active layer.

[61] The third column of plots shows the time evolution of the sorting profile as predicted by the sorting evolution model with regular dunes (model C1). The lower elevation of the active bed equals that of the Hirano model, and sediment fluxes do not occur below this level. Hence the bed composition does not change at these elevations. The time evolution of the sorting profile is similar to the Hirano model, except for the fact that the sorting shows a linear profile within the active part of the bed.

[62] The fourth column of plots shows the time evolution of the sorting profile as predicted by the sorting evolution model with irregular dunes (model C2). Only the latter model and the Ribberink two-layer model are able to modify the composition at the lower elevations. This is due to their wider range of elevations of the active bed, as they account for the effects of the variability in bed form geometry. The sorting profiles at the final stage of the experiment as predicted by these two models agree well with the measured final sorting profile.

4.5. Active Layer Thickness

[63] The thickness of the active layer has appeared to be a crucial factor in large-scale morphodynamic modeling of rivers with nonuniform sediment, as the active layer thickness largely affects the predicted adaptation timescales of, for instance, the rate and composition of the transported sediment. It therefore also strongly affects computed morphodynamic changes. Figure 14 confirms that the active layer thickness largely affects the adaptation timescale of the composition of the transported sediment. From Figure 14 it appears that, using the Hirano model, the active part of the bed is best represented if the active layer thickness is more or less equal to the mean dune height ($\delta = \Delta$), whereas, using the Ribberink two-layer model, the active part of the bed is best represented if $\delta = \frac{1}{2}\Delta$.

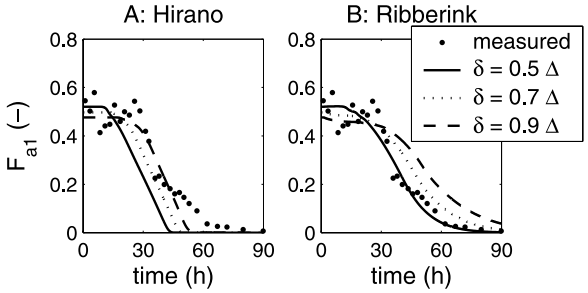

Figure 14. Time evolution of the volume fraction content of the fine size fraction in the transported sediment, F_{a1}, at the downstream end of the flume (x = 28.5 m). Predictions (lines) are from (left) model A, the Hirano active layer model, and (right) model B, the Ribberink two-layer model, wherein the active layer thickness, δ, equals 0.5 Δ, 0.7 Δ, and 0.9 Δ. Measured data (dots) originate from *Ribberink* [1987].

5. Discussion

[64] The specific objective of the present case study is to assess the predictive capacity of submodels for mass conservation. The author has deliberately chosen to keep the other submodels in the morphodynamic model systems as simple as possible and not to provide a model system that is optimally calibrated on the flume experiment. For instance, measured data are used for mean dune height, the PDF of bed form trough elevations, and bed resistance. Another example is that in predicting sediment transport rates we use a sediment transport model that was calibrated against the sediment transport rates as measured in the equilibrium stages of the *Ribberink* [1987] flume experiments. Logically, in predictive river studies such measured data are not available. We then need submodels predicting these parameters.

[65] The present case study stresses the importance of taking into account the variability in bed form geometry in modeling sorting and morphodynamics. The work by *Paola and Borgman* [1991] and *Leclair et al.* [1997] supports this finding by underlining the impact of the irregularity in bed form size on the formation of sedimentary deposits. Although it was not the aim of the present paper, the author expects that a combination of the lee face avalanche submodel by *Blom and Kleinhans* [2006] with a model for cross bedding [e.g., *Leclair*, 2002] may yield interesting results.

[66] The sorting evolution model with regular dunes (model C1) does not improve the computed adaptation

Figure 13. Vertical sorting profile, F_i, at various times during the flume experiment (T′ = 0 h, T = 0 h, T = 10 h, T = 20 h, T = 40 h, and T = 120 h) at the downstream end of the flume (x = 30 m), together with the initial mean bed level at the same position (dotted line) and the predicted mean bed level at time T (dashed line). Predictions (lines) of the volume fraction content of the coarse size fraction, F_{coarse}, over bed elevations are from (left to right) model A, the Hirano active layer model; model B, the Ribberink two-layer model; model C1, the sorting evolution model with regular dunes; and model C2, the sorting evolution model with irregular dunes. The top right plot shows the measured initial sorting profile (data originate from *Ribberink* [1987]). The bottom right plot shows the measured vertical sorting profile relative to the mean bed level at the final state of the experiment (T = 120 h; data originate from *Ribberink* [1987]). The adjustment period T′ covers a period of 5 h in which the model under uniform flow conditions adjusts toward its equilibrium state (section 3.10).

timescales compared to the results of the Hirano active layer model (model A). This shows us that, in reproducing this flume experiment, the introduction of the effects of vertical sorting within an active bed that has a limited thickness does not improve predictions.

[67] All models somewhat underestimate the final amount of aggradation in stage E9, which appears to be due to the fact that the empirical predictors for bed resistance and bed load transport rates are not fully adequate for the conditions of experiment E8-E9 [*Ribberink*, 1987]. Note that an improved prediction of morphodynamics is not only expressed by the improved prediction of net aggradation/degradation in stage E9. An improved prediction of (the time evolution of) vertical sorting and so (the time evolution of) the bed surface composition may strongly contribute to an improved prediction of morphodynamic changes. After all, the bed surface composition is essential in predicting skin friction, bed load and suspended load transport rates, and therefore divergences in the sediment transport rates, and thus net aggradation or degradation. This reasoning would have been illustrated if the present flume experiment were succeeded by a phase of net degradation. Although the flume experiment in question does not enable verifying this statement, the author believes that the improved prediction of the vertical sorting profile and the bed surface composition in stage E9 by models B and C2 would improve the prediction of morphodynamic changes in such a succeeding phase.

[68] Despite showing good results, the Ribberink two-layer model (model B) has some weaknesses. Its formulation for vertical sediment exchange due to the migration of dunes of irregular size is not sufficiently generic for a number of reasons. First, Ribberink specifically calibrated the constants in the sediment exchange term on the flume experiment considered in the present case study. Secondly, the present formulation for the sediment exchange term is only applicable to mixtures of two size fractions. Moreover, the formulation fails in the case that the active layer consists mostly of the fine size fraction; in this case mass is not conserved. Finally, the set of equations still potentially becomes elliptic.

[69] Despite showing good results, the sorting evolution model (model C2) has some weaknesses, as well. Application of the model has appeared to be cumbersome. The adaptation of the sorting profile happens infinitely fast at the uppermost elevations of the active part of the bed, which leads to numerical problems. In the computations we therefore do not consider the 3% highest elevations within the series of (irregular) bed forms (Figure 7). Still, the time step needs to be very small (20 s) in order to prevent the volume fraction content of size fractions from becoming smaller than 0 or exceeding 1 at all active elevations. For this reason, the computational time is much larger than the computational time using the Hirano or Ribberink bed layer models. Another point is that application of the sorting evolution model requires knowledge about the PDF of relative trough elevations. Although this requirement asks for additional information compared to the Hirano and Ribberink bed layer models, the author would not characterize this as a weakness for the following two reasons. The first reason is that modeling the active part of the bed as a stochastic (set of) parameter(s) rather than a discrete and homogeneous bed layer offers a much better representation of the active part of the bed. The second reason is that an external submodel for the PDF of relative trough elevations is available. *Van der Mark et al.* [2007] have shown that the PDF of relative trough elevations is well described using a Weibull distribution (i.e., a longer tail for the higher relative trough elevations or, in other words, for the deeper troughs), in which the standard deviation of relative trough elevation is a simple linear function of the mean relative trough elevation.

[70] Noteworthy is that *Ribberink* [1987] found that application of the Hirano model to the present flume experiment led to instability (ellipticity) of the model. This instability was not found in the present case study. This may be due to the different numerical schemes and/or to the fact that in the present study a detailed bookkeeping system is applied for registering the volume fraction content of size fractions at elevations within the active and inactive part of the bed.

[71] Morphodynamic modeling of rivers dominated by nonuniform sediment is governed by the interplay between submodels for: (1) the grain size–selective sediment transport; (2) mass conservation of nonuniform sediment including sediment fluxes within the bed; (3) the composition of the bed surface (also see next paragraph); (4) the range of bed elevations exposed to the flow (i.e., the range of active elevations); (5) skin friction (based on the bed surface composition); and (6) form drag (based on the PDF of bed surface elevations). The fact that previous research on morphodynamic modeling of rivers governed by nonuniform sediment has often led to disappointing results has made people try to improve grain size–selective sediment transport models (submodel no. 1 from the above list). However, the disappointing results need not arise from the grain size–selective sediment transport model and may well be caused by shortcomings in the other models mentioned above.

[72] A generally neglected topic is the submodel for the mean composition of the bed surface, F_{suri} (section 3). This parameter is derived from the computed vertical sorting profile and is used for calculating skin friction and grain size–selective sediment transport rates. In order to find an adequate model for the mean composition of the bed surface, the question to be asked is "Which part of the bed determines skin friction and which part of the bed determines the grain size–selective sediment transport rates?" One has to realize that the method to determine the mean composition of the bed surface needs to suit the specific submodels applied in calculating the hydraulic roughness, grain size–selective bed load transport, and grain size–selective suspended load transport.

[73] As application of the Ribberink two-layer model or the sorting evolution model accounting for variability in bed form size appears to be problematic, present work by the author focuses on the development of a new bed layer–type model that takes into account the variability in bed form geometry, and wherein formulations for vertical sediment fluxes derived from the sorting evolution model are also incorporated. The discretization of the active part of the bed into multiple bed layers is based on the probability density function of active bed elevations, which is based on the findings by *Van der Mark et al.* [2007]. As the timescale of the adaptation of the vertical sorting profile is small for the

upper elevations of the active part of the bed, we can usefully apply the equilibrium sorting approach [*Blom et al.*, 2006] to these elevations. Formulations for the sediment fluxes between the discrete bed layers are derived from the sorting evolution model.

6. Conclusions

[74] This paper presents the results of a case study in which four sediment continuity models are each incorporated in a morphodynamic model system and applied to simulate the aggradational flume experiment conducted by *Ribberink* [1987]. The case study shows that taking into account the variability in bed form geometry largely improves the prediction of the adaptation timescales of various physical parameters, e.g., the bed surface composition, the vertical sorting profile, and the composition of the bed load transport. This is because it allows sediment to be "stored" (temporarily) at elevations where the sediment is exposed to the flow less frequently than at higher elevations.

[75] The *Ribberink* [1987] two-layer model and the *Blom et al.* [2008] sorting evolution model include the effects of variability in bed form geometry in modeling large-scale morphodynamics and show good results in simulating the flume experiment in question.

[76] Both models, however, suffer from a number of shortcomings. The Ribberink two-layer model is not sufficiently generic as (1) its vertical sediment exchange term was calibrated on the flume experiment in question; (2) the sediment exchange term is yet suitable for sediment mixtures composed of two size fractions only; (3) under some conditions the sediment exchange term does not conserve mass; and (4) the elliptic character of the set of equations is not eliminated completely (although the probability of becoming elliptic appears to be small). Application of the sorting evolution model is cumbersome as it requires a small numerical time step. The sorting evolution model requires information on the probability density function of relative trough elevations, which can be provided from an external submodel [*Van der Mark et al.*, 2007].

[77] Using the *Hirano* [1971] model, the active part of the bed appears to be best represented if the active layer thickness is more or less equal to the mean dune height, whereas the *Ribberink* [1987] two-layer model shows better results if the active layer thickness is set equal to more or less half the mean dune height.

[78] Future application to large-scale field cases asks for the development of a new bed layer–type model that takes into account the variability in bed form geometry, and wherein formulations for vertical sediment fluxes derived from the sorting evolution model are also incorporated.

Appendix A: Model A: Hirano Active Layer Model

[79] *Hirano* [1970, 1971, 1972] divides the bed into a homogeneous top layer, i.e., the active layer, and a nonmoving homogeneous substrate (Figure A1). In the *Hirano* [1971] active layer model, conservation of mass is guaranteed if

$$c_b \frac{\partial (F_{mi}\,\delta)}{\partial t} + c_b\, F_{L1,i} \frac{\partial \eta_{L1}}{\partial t} = -\frac{\partial (F_{ai}\, q_a)}{\partial x} \tag{A1}$$

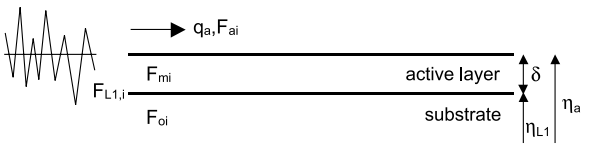

Figure A1. *Hirano* [1971] active layer model, revised from *Hirano* [1971, Figure 2].

which is valid for all grain size fractions $i = 1, .., N$, where i denotes the specific grain size fraction. The parameters t and x denote the time coordinate and streamwise coordinate, respectively, c_b denotes the concentration of sediment in the bed ($c_b = 1 - \lambda_b$, where λ_b denotes the porosity), δ denotes the thickness of the active layer, η_{L1} denotes the elevation of the interface between the active layer and the substrate, F_{mi} denotes the volume fraction content of size fraction i in the active layer, $F_{L1,i}$ denotes the volume fraction content of size fraction i in the sediment flux between the active layer and the substrate, q_a denotes the volume of transported sediment per unit width and time, F_{ai} denotes the volume fraction content of size fraction i in the transported sediment ($F_{ai} = q_{ai}/q_a$, where q_{ai} denotes the volume of transported sediment of size fraction i per unit width and time).

[80] If the elevation of the interface rises ($\partial \eta_{L1}/\partial t > 0$), the volume fraction content of size fraction i in the sediment flux between the active layer and the substrate, $F_{L1,i}$, equals the volume fraction content of size fraction i in the active layer, F_{mi}. If the elevation of the interface lowers ($\partial \eta_{L1}/\partial t < 0$), $F_{L1,i}$ equals the volume fraction content of size fraction i in the substrate, F_{oi}:

$$F_{L1,i} = \begin{cases} F_{mi} & \text{if } \partial \eta_{L1}/\partial t > 0 \\ F_{oi} & \text{if } \partial \eta_{L1}/\partial t < 0 \end{cases} \tag{A2}$$

[81] In plane-bed conditions, we typically assume the active layer thickness, δ, equal to some coarse grain size in the mixture (e.g., $\delta = d_{90}$ where d_{90} denotes the grain size for which 90% of the mixture is finer). In conditions with bed forms, we typically relate the active layer thickness to the mean bed form height, e.g., $\delta = \frac{1}{2}\Delta$ where Δ denotes the mean bed form height [*Ribberink*, 1987; *Armanini and Di Silvio*, 1988; *Parker*, 1991]. *Kelsey* [1996] provides an overview of definitions of the active layer thickness.

[82] Solving the time evolution of the volume fraction content of size fraction i in the active layer, F_{mi}, from equation (A1) requires the time evolution of the elevation of the interface between the active layer and the substrate, η_{L1}, to be known. We compute the elevation of the interface from

$$\eta_{L1} = \eta_a - \delta \tag{A3}$$

(also see Figure A1). Note that in most cases both quantities on the right-hand side of equation (A3) are time dependent. We compute the time evolution of the mean bed level, η_a, from

$$c_b \frac{\eta_a}{\partial t} = -\frac{\partial q_a}{\partial x} \tag{A4}$$

where $q_a = \sum_i^N q_{ai}$, and we compute the time evolution of the sediment transport rate of size fraction i, q_{ai}, using a submodel

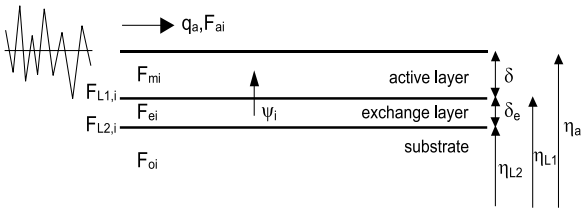

Figure B1. *Ribberink* [1987] two-layer model, revised from *Ribberink* [1987, Figure 4.3].

for grain size–selective sediment transport. In equation (A3), the thickness of the active layer, δ, may well also be time dependent as it depends on flow strength. On the basis of flume experiments under plane bed conditions, *Wong Egoavil* [2006] finds that the range of active elevations increases with increasing flow strength. Under conditions with dunes, dune height (and therefore the range of active elevations) increases with increasing flow strength, up until dune washout and subsequent upper regime plane bed conditions are reached.

Appendix B: Model B: Ribberink Two-Layer Model

[83] *Ribberink* [1987] introduces an additional layer in his two-layer model below the active layer, i.e., the exchange layer (Figure B1). This exchange layer represents the bed elevations that become exposed to the flow by occasionally deep bed form troughs. The vertical sediment exchange flux, ψ_i, in Figure B1 represents vertical sediment fluxes induced by these deep bed form troughs. Conservation of mass for the active layer and the exchange layer now yields

$$c_b \frac{\partial (F_{mi}\delta)}{\partial t} + c_b F_{L1,i} \frac{\partial \eta_{L1}}{\partial t} = \psi_i - \frac{\partial (F_{ai}\, q_a)}{\partial x} \tag{B1}$$

$$c_b \frac{\partial (F_{ei}\delta_e)}{\partial t} + c_b F_{L2,i} \frac{\partial \eta_{L2}}{\partial t} - c_b F_{L1,i} \frac{\partial \eta_{L1}}{\partial t} = -\psi_i \tag{B2}$$

which is valid for all grain size fractions $i = 1, .., N$. Here δ_e denotes the thickness of the exchange layer, η_{L1} now denotes the elevation of the interface between the active layer and the exchange layer, η_{L2} denotes the elevation of the interface between the exchange layer and the substrate, F_{ei} denotes the volume fraction content of size fraction i in the exchange layer, $F_{L1,i}$ denotes the volume fraction content of size fraction i at the interface between the active layer and the exchange layer, and $F_{L2,i}$ denotes the volume fraction content of size fraction i at the interface between the exchange layer and the substrate. *Ribberink* [1987] provides a detailed description of the vertical sediment exchange flux due to occasionally deep bed form troughs, ψ_i.

[84] We compute the time evolution of the elevation of the interface between the active layer and the exchange layer, η_{L1}, from equation (A3), and the time evolution of the elevation of the interface between the exchange layer and the substrate, η_{L2}, from

$$\eta_{L2} = \eta_a - \delta - \delta_e \tag{B3}$$

where all terms at the right-hand side are usually time-dependent. We compute the time evolution of the mean bed level, η_a, from equation (A4). On the basis of his flume experiments [*Ribberink*, 1987] defines the exchange layer thickness, δ_e, to be a function of the active layer thickness, δ ($\delta_e = 1.22\delta$).

[85] If the elevation of the interface between the active layer and the exchange layer rises ($\partial\eta_{L1}/\partial t > 0$), a sediment flux occurs from the active layer to the exchange layer and the volume fraction content of size fraction i at this interface, $F_{L1,i}$, equals the volume fraction content of size fraction i in the active layer, F_{mi}. If the interface lowers ($\partial\eta_{L1}/\partial t < 0$), $F_{L1,i}$ equals the volume fraction content of size fraction i in the exchange layer, F_{ei}. We apply a similar approach to the bed composition at the elevation of the interface between the exchange layer and the substrate, $F_{L2,i}$:

$$F_{L1,i} = \begin{cases} F_{mi} & \text{if } \partial\eta_{L1}/\partial t > 0 \\ F_{ei} & \text{if } \partial\eta_{L1}/\partial t < 0 \end{cases} \tag{B4}$$

$$F_{L2,i} = \begin{cases} F_{ei} & \text{if } \partial\eta_{L2}/\partial t > 0 \\ F_{oi} & \text{if } \partial\eta_{L2}/\partial t < 0 \end{cases} \tag{B5}$$

[86] Mathematical analysis indicates that the two-layer model does not completely avoid ellipticity of its set of equations [*Ribberink*, 1987]. However, the probability of becoming elliptic is significantly smaller than for the active layer model, as the two-layer model generally tends toward a situation in which the mean grain size of the active layer is smaller than that of the exchange layer. Note that *Ribberink* [1987] already applied the Hirano and Ribberink bed layer models to the flume experiment considered in the present paper. Ribberink calibrated his two-layer model explicitly on this flume experiment. The Hirano active layer model appeared incapable of describing the slow adaptation of the composition of the active layer and the bed load transport composition, while the calibrated [*Ribberink*, 1987] two-layer model showed much better results.

Appendix C: Model C: *Blom et al.* [2008] Sorting Evolution Model

[87] The sorting evolution model developed by *Blom et al.* [2008] takes into account the variability in bed form geometry by accounting for the PDF of bed form trough elevations. In the sorting evolution model, conservation of mass is guaranteed if

$$\frac{\partial C_i}{\partial t} = D_{ei} - E_{ei} \tag{C1}$$

where C_i denotes the concentration of size fraction i at elevation z ($C_i = c_b P_s F_i$). Note that all parameters are averaged over a reach covering a large number of bed forms. F_i denotes the volume fraction content of size fraction i at elevation z, P_s denotes the probability distribution of bed surface elevations indicating the probability that the bed surface elevation is higher than z, D_{ei} denotes the deposition density of size fraction i defined such that $D_{ei}dxdz$ is the volume of sediment of

size fraction i that is deposited per unit width and time in a bed element with sides dx and dz at elevation z, and, likewise, E_{ei} denotes the entrainment density of size fraction i.

[88] The sorting evolution model distinguishes three types of vertical sediment flux: sediment fluxes through dune migration, i.e., grain size–selective deposition down the lee faces of (irregular) bed forms (type I); sediment fluxes through a change in time of the PDF of relative trough elevations (type II); and sediment fluxes through net aggradation or degradation (type III). Assuming a constant and uniform porosity, we rewrite equation (C1) to

$$c_b \frac{\partial (P_s F_i)}{\partial t} = (D_{ei} - E_{ei})|_I + (D_{ei} - E_{ei})|_{II} + (D_{ei} - E_{ei})|_{III} \quad \text{(C2)}$$

Blom et al. [2008] provide a further elaboration of equation (C2) and a satisfactory test of the formulations for sediment fluxes of type I and II. In the present case study, the formulations for sediment fluxes of type I are based on the lee face avalanche submodel proposed by *Blom and Kleinhans* [2006]. In the present paper we apply the formulations for sediment fluxes through net aggradation or degradation (type III) for the first time.

[89] **Acknowledgments.** This research is supported by the Technology Foundation STW, applied science division of the Netherlands Organisation for Scientific Research (NWO) and the technology programme of the Ministry of Economic Affairs (VENI grant TCB.6286), as well as by the STC program of the National Science Foundation via the U.S. National Center for Earth-surface Dynamics (NCED) under agreement EAR-0120914. More specifically, this paper addresses NCED's research efforts on channels and stream restoration. The author wishes to acknowledge NCED for enabling the joint research between the author and Gary Parker (University of Illinois at Urbana-Champaign). The author thanks Jan S. Ribberink for sharing insightful details of the flume experiment and fruitful discussion of the model results, Gary Parker for stimulating discussions and joint work during a 2 months' visit by the author to the St. Anthony Falls Laboratory in 2004, and Bert Jagers of Deltares for providing part of the measured data of the flume experiment in digital format.

References

Allen, J. R. L. (1965), Sedimentation to the lee of small underwater sand waves: An experimental study, *J. Geol.*, *73*, 95–116.

Armanini, A. (1995), Non-uniform sediment transport: Dynamics of the active layer, *J. Hydraul. Res.*, *33*(5), 611–622.

Armanini, A., and G. Di Silvio (1988), A one-dimensional model for the transport of a sediment mixture in non-equilibrium conditions, *J. Hydraul. Res.*, *26*(3), 275–292.

Bagnold, R. A. (1941), *The Physics of Blown Sand and Desert Dunes*, Methuen, New York.

Blom, A., and M. G. Kleinhans (2006), Modelling sorting over the lee face of individual bed forms, in *River Flow 2006: Proceedings of the International Conference on Fluvial Hydraulics*, edited by R. M. L. Ferreira et al., pp. 807–816, Taylor and Francis, Leiden, Netherlands.

Blom, A., and G. Parker (2004), Vertical sorting and the morphodynamics of bed form-dominated rivers: A modeling framework, *J. Geophys. Res.*, *109*, F02007, doi:10.1029/2003JF000069.

Blom, A., J. S. Ribberink, and H. J. de Vriend (2003), Vertical sorting in bed forms: Flume experiments with a natural and a trimodal sediment mixture, *Water Resour. Res.*, *39*(2), 1025, doi:10.1029/2001WR001088.

Blom, A., G. Parker, J. S. Ribberink, and H. J. de Vriend (2006), Vertical sorting and the morphodynamics of bed-form-dominated rivers: An equilibrium sorting model, *J. Geophys. Res.*, *111*, F01006, doi:10.1029/2004JF000175.

Blom, A., J. S. Ribberink, and G. Parker (2008), Vertical sorting and the morphodynamics of bed form–dominated rivers: A sorting evolution model, *J. Geophys. Res.*, doi:10.1029/2006JF000618, in press.

Crickmore, M. J., and G. H. Lean (1962a), The measurement of sand transport by means of radioactive tracers, *Proc. R. Soc. London, Ser. A*, *266*, 402–421.

Crickmore, M. J., and G. H. Lean (1962b), The measurement of sand transport by the time-integration method with radioactive tracers, *Proc. R. Soc. London, Ser. A*, *270*, 27–47.

Egiazaroff, I. V. (1965), Calculation of nonuniform sediment concentrations, *J. Hydraul. Div. Am. Soc. Civ. Eng.*, *91*(HY4), 225–248.

Gilbert, G. K. (1914), The transportation of debris by running water, *U.S. Geol. Surv. Prof. Pap.*, *86*, 263 pp.

Hirano, M. (1970), On phenomena of river-bed lowering and armouring below reservoirs, paper presented at 14th Hydraulics Lecture Meeting, Civ. Eng. Assoc. Hydraul. Comm., Tokyo, 13–14 Feb.

Hirano, M. (1971), River bed degradation with armouring, *Trans. Jpn. Soc. Civ. Eng.*, *3*, 194–195.

Hirano, M. (1972), Studies on variation and equilibrium state of a river bed composed of nonuniform material, *Trans. Jpn. Soc. Civ. Eng.*, *4*, 128–129.

Hotchkiss, R. H., and G. Parker (1991), Shock fitting of aggradational profiles due to backwater, *J. Hydraul. Eng.*, *117*(9), 1129–1144.

Ikeda, H., and F. Iseya (1988), Experimental study of heterogeneous sediment transport, *Environ. Res. Cent. Pap. 12*, Univ. of Tsukuba, Tsukuba, Japan.

Kelsey, A. (1996), Modelling the sediment transport process, in *Advances in Fluvial Dynamics and Stratigraphy*, edited by P. A. Carling and M. R. Dawson, pp. 229–261, John Wiley, Chicester, U. K.

Knighton, A. D. (1998), *Fluvial Forms and Processes: A New Perspective*, Edward Arnold, London.

Leclair, S. F. (2002), Preservation of cross-strata due to the migration of subaqueous dunes: An experimental investigation, *Sedimentology*, *49*, 1157–1180.

Leclair, S. F., J. S. Bridge, and F. Wang (1997), Preservation of cross-strata due to migration of subaqueous dunes over aggrading and non-aggrading beds: Comparison of experimental data with theory, *Geosci. Can.*, *24*, 55–66.

Meyer-Peter, E., and R. Müller (1948), Formulas for bed-load transport, paper presented at 2nd Meeting, Int. Assoc. Hydraul. Res., Stockholm.

Paola, C., and L. Borgman (1991), Reconstructing random topography from preserved stratification, *Sedimentology*, *38*, 553–565.

Parker, G. (1991), Selective sorting and abrasion of river gravel. I. Theory, *J. Hydraul. Eng.*, *117*(2), 113–149.

Parker, G., C. Paola, and S. F. Leclair (2000), Probabilistic Exner sediment continuity equation for mixtures with no active layer, *J. Hydraul. Eng.*, *126*(11), 818–826.

Ribberink, J. S. (1987), Mathematical modelling of one-dimensional morphological changes in rivers with non-uniform sediment, Ph.D. thesis, Delft Univ. of Technol., Delft, Netherlands.

Van der Mark, C. F., A. Blom, and S. J. M. H. Hulscher (2007), Variability in bedform characteristics using flume and river data, in *River, Coastal and Estuarine Morphodynamics: RCEM 2007*, edited by C. M. Dohmen-Janssen and S. J. M. H. Hulscher, pp. 923–930, Taylor and Francis, London.

Wilcock, P. R., and J. C. Crowe (2003), Surface-based transport model for mixed-size sediment, *J. Hydraul. Eng.*, *129*(2), 120–128.

Wong Egoavil, M. (2006), Model for erosion, transport and deposition of tracer stones in gravel-bed streams, Ph.D. thesis, Univ. of Minn., Minneapolis.

Zanke, U. (1976), Über den Einfluss von Kornmaterial, Strömungen und Wasserstanden auf die Korngrossen von Transportkörpern in offenen Gerinnen (in German), *Tech. Rep. 44*, Mitt. Franzius Inst., Hannover, Germany.

A. Blom, Environmental Fluid Mechanics Section, Civil Engineering and Geosciences, Delft University of Technology, P.O. Box 5048, NL-2628 CN Delft, Netherlands. (astrid.blom@tudelft.nl)